Exploring Deposition Temperature-Tailored Structural and Morphological Transformations in Electrochemically Deposited PbOx on Cu Substrate with Acetate-Electrolyte

Parvaj Rana[1], Pradip Kumar Biswas[2], Samia Tabassum[3], Ferdous Rahman[4], Abu Bakar Md. Ismail[1]*

[1]*Solar Energy Lab, Department of Electrical and Electronic Engineering, University of Rajshahi, Rajshahi 6205, Bangladesh.*
[2]*Institute of Mining, Mineralogy & Metallurgy, Bangladesh Council of Scientific and Industrial Research (BCSIR), Joypurhat-5900, Bangladesh.*
[3]*Institute of Energy Research and Development (IERD), Bangladesh Council of Scientific and Industrial Research (BCSIR), Dhaka*
[4]*Department of Electrical & Electronic Engineering, Begum Rokeya University, Rangpur, Bangladesh.*
*Corresponding author, Email address: rubon.abm.ismail@gmail.com

Abstract: The electrolyte type and its temperature affect different characteristics of the metal oxides deposited through electrochemical processes. This paper examines how acetate electrolytes affect the crystallite properties, composition, and morphology of electrochemically deposited Lead Oxide (PbOx) on a copper (Cu) substrate, depending on the deposition temperature of the electrolytic bath. The PbO_x film was deposited from the aqueous solution of Lead (II) acetate trihydrate $(Pb(C_2H_3O_2)_2.3H_2O)$ and sodium nitrate $(NaNO_3)$ at pH-3 where the deposition was performed at an electrolyte temperature of 30˚C, 60˚C, and 80˚C respectively. XRD spectra revealed that both PbO and PbO_2 were present with α, and β phase compositions. It is found that crystallite size (D) attains a maximum value of about 22.64 nm at a deposition temperature of 80˚C, where interplaner spacing, dislocation density, and micro-strain possess a minimum value. The EDAX analysis yielded similar results, indicating that increasing the deposition temperature increased the quantity of oxygen (O) present in the deposited films. Again, the mass (%) and atom (%) ratios of lead (Pb) and O decreased as the deposition temperature increased. The SEM study showed a stellar, densely minutely tuberculate structure with a flat Centre structure of deposited PbOx layers at low temperatures. At 80˚C deposition temperature, the stellar structure of deposited films transformed into the fractal structure. All these experimental facts indicate that the deposition temperature can be a tool for tailoring the structural and morphological properties of Electrochemically deposited PbOx from acetate electrolyte.

1. Introduction

Solid oxide electrodes find wide applications in various fields such as industrial wastewater treatment, sonoelectrochemistry, and photoelectrochemistry (Sáez *et al.*, 2011). Lead Oxide (PbO₂) stands out as a popular solid oxide, initially employed as a positive electrode in lead acid batteries (Chen *et al.*, 2013), (Zhao *et al.*, 2018). PbO₂ is also utilized in industrial processes for the production

of ozone, perchlorate, and chromates (Pletcher *et al.*, 1993). Its cost-effectiveness compared to noble metals, ease of preparation, excellent electrical conductivity, chemical stability in corrosive environments, substantial surface area, and significant over-potential for the oxygen evolution reaction make PbO_2 suitable for industrial and electrochemical applications. It serves as an anodic material for ozone production (Pletcher *et al.*, 1993), (Stucki *et al.*, 1985), (Kinoshita *et al.*, 1992), an electro-catalyst for the formation of salicylic acid and 2-naphthol (Ai *et al.*, 2005, Panizza *et al.*, 2003), in wastewater treatment (Devilliers *et al.*, 2003), (Johnson *et al.*, 2000), (Tong *et al.*, 2008) and as a pH sensor (Eftkhari *et al.*, 2003). Recently, PbO_2 has been explored as the starting material for creating organometal perovskite for use as the absorber material in solar cells (Al Katrib *et al.*, 2021). Despite its advantages, PbO_2 requires improvements in stability and electrocatalytic activity (Labiadh *et al.*, 2016). Researchers are exploring the choice of substrate and its modification to address this issue (Elaissaoui *et al.*, 2018), (Duan *et al.*, 2017).

PbO can be produced using various vacuum techniques like molecular beam epitaxy and sputtering (Boubatra *et al.*, 2011). However, an alternative method for synthesizing PbO is electrochemical deposition, which offers advantages such as low cost, simplicity, versatility, scalability, and compatibility with roll-to-roll manufacturing (Boubatra *et al.*, 2011), (Chen *et al.*, 2015). In electrochemical deposition, factors like deposition temperature, solvent, film-substrate interaction, and solution concentration directly influence the morphology, growth mechanism, and crystal properties (Salim *et al.*, 2015). The choice of electrolyte also plays a crucial role in determining the morphology of the electrodeposited films (Nikolic´ *et al.*, 2015). The majority of electrodeposition processes were carried out using nitrate electrolytes. Previous studies have explored how different deposition parameters affect the properties of PbO_2 on Nickel and Carbon substrates (Hossain *et al.*, 2017), (Blood *et al.*, 2004). Metals and metal oxides like Nickel, Copper, TiO_2, and Fe_2Se_2 have been widely researched for the impact of pH and deposition temperature on the electrodeposited film (Boubatra *et al.*, 2011), (Nikolić *et al.*, 2007), (Mahalingam *et al.*, 2007), (Tang *et al.*, 2005). However, the effect of acetate electrolyte temperature on the structural and morphological properties of electrochemically deposited PbOx has been rarely explored. Under this background, we investigate the influence of acetate electrolyte bath temperature on the electrodeposition of PbOx film on the Cu substrate from an aqueous acetate electrolyte. The deposition was carried out at temperatures of 30˚C, 60˚C, and 80˚C, and the impact of deposition temperature on crystalline properties, composition, and morphological structure has been examined and reported. Experimental results suggest that the deposition temperature could effectively adjust the various properties of electrochemically deposited lead oxide on Cu substrate from an acetate electrolyte.

2. Methodology

2.1 Experiments

The PbOx film was deposited on a properly cleaned Cu substrate from an aqueous solution containing 0.025M lead (II) acetate trihydrate and 0.05M sodium nitrate, with the precursor solution's pH around 3. During the preparation of the precursor solution, it was stirred using a NanBel magnetic stirrer-model: MS 300 and heated to approximately 50˚C. The initial pH of the prepared precursor solution was 5.2, which was then adjusted to 3 by adding acetic acid. Prior to deposition, both the substrates and electrodes underwent a cleaning process involving distilled water for 5 minutes, followed by acetone for another 5 minutes, and finally rinsed in distilled water for an additional 5 minutes. The electrodeposition process was carried out using Admiral-squidstat plus and controlled by a personal computer. A three-electrode configuration was utilized for the PbOx deposition, with Cu

substrate, Pt, and AgCl/Ag serving as working, counter, and reference electrodes respectively. The depositions took place at bath temperatures of 30˚C, 60˚C, and 80˚C, each lasting 4 minutes. Subsequently, the deposited films underwent annealing at around 70˚C. X-ray diffraction analysis of the deposited films was performed using the GBC-XRD Emma diffractometer with Cu kα radiation. The XRD measurements were analyzed using the Match software provided by Crystal Impact and OriginPro 2018 software. Parameters such as average crystalline size, interplanar spacing, dislocation density, and microstrain of the deposited films were calculated. The compositional structure and surface morphology were evaluated using a scanning electron microscope and an energy dispersive X-ray analysis setup (EDAX) attached to the ZEISS FESEM SIGMA-300.

2.3 Product characterisation

The products (biomass biochar and hybrid biochar) recovered from the process were characterised to ascertain some of their properties using Scanning Electron Microscope with energy Dispersive X-ray Spectroscopy (SEM-EDS), Fourier Transform Infra-Red Spectroscopy (FTIR) and Brunauer-Emmet-Teller (BET) analysis. Scanning Electron Microscopy (SEM, Phenom proX, Phenom-World BV, Netherlands) was used to study the surface morphology of the particles of the biochar. A double adhesive was placed on a sample stub. The sample was sprinkled on the sample stub and subsequently taken to a sputter coater (quorum-Q150R Plus E) and coated with 5 nm of gold. The sample was placed on a charge reduction sample holder and introduced into the column of the SEM machine. It was firstly viewed with a NavCam before being sent to SEM mode. The acceleration voltage of the microscope was set to 15 kV and magnification at 1000 – 1500×. FTIR (Shimadzu, FTIR-8400S, Japan) was used to determine the functional groups and complexes present in both biochar samples. The surface area, pore volume and size of the chars were measured. The surface properties of the char samples were studied using a Multipoint BET surface area and the DR (Dubinin–Radushkevic) method for the pore volume and width (diameter). Adsorbate was introduced to give the lowest desired relative pressure, and then the volume adsorbed was measured.

3. Results and Discussion

3.1 Structural Studies

The X-ray diffraction report clearly demonstrates the impact of varying deposition temperature on the crystalline properties of the deposited films. X-ray diffraction patterns for the films deposited on Cu substrate at different temperatures (30˚C, 60˚C, and 80˚C) are illustrated in **Figure 1**. It is evident from the diffractograms that the deposited PbOx exhibits a polycrystalline nature, with new diffraction peaks emerging more prominently as the deposition temperature rises. The phase compositions α and β of PbO and PbO$_2$ are also identified (Chen *et al.*, 2013), (Zhao *et al.*, 2018), (Hossain *et al.*, 2017), (Stillman *et al.*, 1984). Furthermore, a prominent peak is observed at around 2θ value of 50.20 degrees, along with some diffraction peaks attributed to the Cu substrate used as a working electrode.

The structural parameters of films deposited at three different temperatures were determined through XRD analysis. The interplanar spacing (d) is calculated using Bragg's Diffraction Law (Kocyigit *et al.*, 2019) as follows:

$$n\lambda = 2d\sin\theta \qquad \text{----} \qquad \text{----} \qquad \text{----} \qquad \textbf{Eqn. 1}$$

where n is an integer typically considered as unity, λ represents the incident wavelength, θ is Bragg's diffraction angle, and d signifies interplanar spacing. The interplanar spacing of deposited films is

detailed in **Table-1**. The crystallite size (D) is determined using Scherrer's equation based on the most prominent diffraction peaks, as shown in **Eqn. 2.** Additionally, the geometric discrepancies between the substrate and deposited film, such as dislocation density (δ) and micro-strain (€), are calculated and presented in **Table-1**. The dislocation density (δ) and micro-strain (€) are computed using **Eqn. 3** and **Eqn. 4**, respectively (Kocyigit *et al.*, 2019).

$$D = \frac{0.9\lambda}{\beta cos\theta} \qquad ---- \qquad ---- \qquad ---- \qquad \textbf{Eqn. 2}$$

$$\delta = \frac{1}{D^2} \qquad ---- \qquad ---- \qquad ---- \qquad \textbf{Eqn. 3}$$

$$€ = \left(\frac{1}{sin\theta}\right)\left[\left(\frac{\lambda}{D}\right) - (\beta \, cos\theta)\right] \qquad ---- \qquad ---- \qquad ---- \qquad \textbf{Eqn. 4}$$

β is the full width at the maximum peak (FWHM) of diffraction peaks.
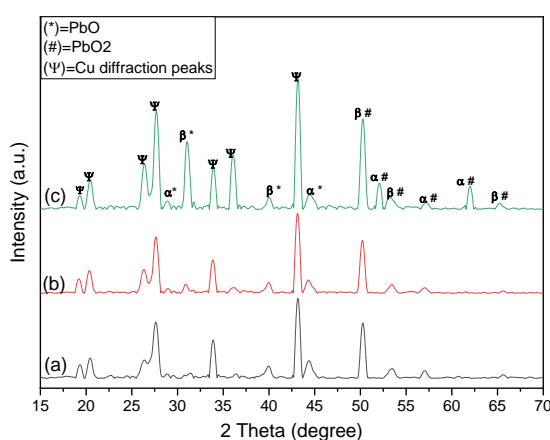
Figure 1. X-ray diffractograms of PbOx deposited at (a) 30˚C (b) 60˚C (c) 80˚C temperature.
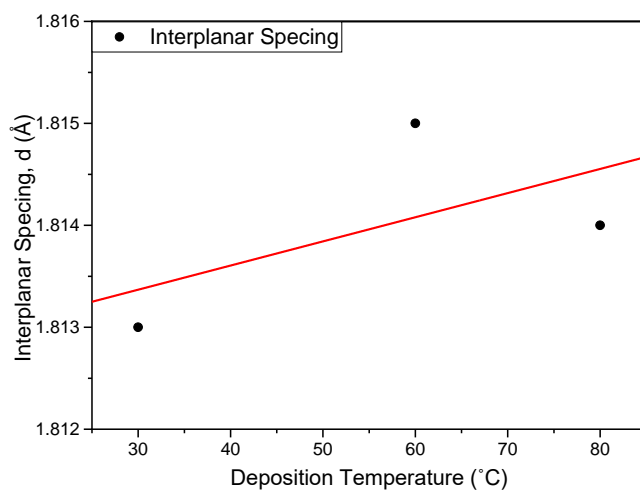
Figure 2. The variation of interplanar spacing of PbOx films deposited at 30˚C, 60˚C, and 80˚C temperature.

To investigate the impact of varying the deposition temperature on crystallite size, interplanar spacing, and dislocation density, we analyze the prominent peak at approximately 2θ value of 50.20 degrees. The interplanar spacing shows minimal increase when the temperature is raised from 30 to 60˚C, but then decreases slightly when the deposition temperature is further increased to 80˚C, as illustrated in **Figure 2**. This phenomenon may be attributed to the influence of substrate temperature on the growth mechanism (Suganya *et al.*, 2014).

Table 1. The structural parameters of PbOx films deposited at 30℃, 60℃, at 80℃ temperature.

Deposition temperature	Phase Composition	Pick Position, 2θ (**Degree**)	FWHM (**Degree**)	Inter-planar Spacing d, (Å)	Crystalline Size, D (nm)	Dislocation Density, δ $(\times 10^{15})$(lines/m^2)	Micro-strain, $\in$ (**x10^{-3}**)
30˚C	α-PbO	27.62	0.7156	3.2270	11.4316	7.6522	5.6458
	β-PbO	31.42	0.6501	2.8449	12.6931	6.2067	4.4825
	β-PbO	39.98	0.7157	2.2533	11.8105	7.1691	3.8157
	α-PbO	43.1	0.5719	2.0971	14.9350	4.4832	2.8083
	β-PbO$_2$	50.28	0.5854	1.8132	14.9902	4.4502	2.4191
	β- PbO$_2$	53.44	0.844	1.7132	10.5380	9.0051	3.2514
	α- PbO$_2$	57.04	0.6409	1.6133	14.1075	5.0246	2.2871
60˚C	α-PbO	28.96	0.5177	3.0807	15.8482	3.9815	3.8877
	β-PbO	30.88	0.5291	2.8934	15.5760	4.1218	3.7152
	β-PbO	39.98	0.6319	2.2533	13.3776	5.5878	3.3687
	α-PbO	43.12	0.5778	2.0962	14.7833	4.5757	2.8359
	β- PbO$_2$	50.22	0.5974	1.8152	14.6863	4.6364	2.4720
	β- PbO$_2$	53.44	0.7973	1.7132	11.1552	8.0361	3.0715
	α- PbO$_2$	57	0.7755	1.6143	11.6571	7.3590	2.7697
80˚C	α-PbO	27.74	0.3134	3.2133	26.1059	1.4673	2.4618
	β-PbO	31.14	0.2129	2.8698	38.7270	0.6667	1.4821
	β-PbO	40.1	0.5199	2.2468	16.2663	3.7794	2.7626
	α-PbO	43.1	0.2922	2.0971	29.2312	1.1703	1.4349
	β- PbO$_2$	50.24	0.3875	1.8145	22.6429	1.9504	1.6027
	α- PbO$_2$	52.06	0.2564	1.7553	34.4709	0.84158	1.0184
	β- PbO$_2$	53.1	1.068	1.7233	8.3154	14.462	4.1450
	α- PbO$_2$	57.04	0.845	1.6133	10.7000	8.7345	3.0155
	α- PbO$_2$	61.96	0.3128	1.4965	29.6222	1.1396	1.0104
	β- PbO$_2$	65.06	0.3836	1.4325	24.5578	1.6581	1.1666
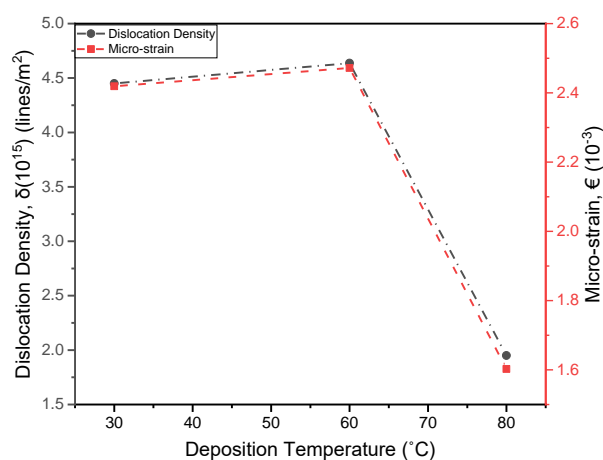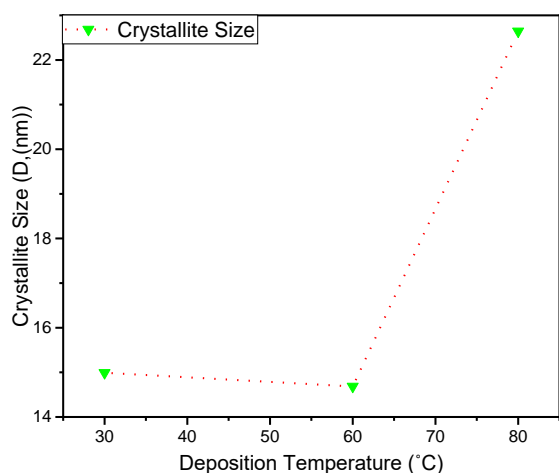
Figure 3a. Variation crystallite size and **3b**. variation of dislocation density and micro-strain of PbOx films

The variation of crystallite size with the deposition temperature for PbOx films is illustrated in **Figure 3a**. **Figure 3b** shows the variation of dislocation density and micro-strain with the deposition temperature. It is noted from **Figure 3a** that initially, as the deposition temperature is raised from 30 to 60°C, the crystallite size decreases from 14.9902 nm to 14.6862 nm. However, upon reaching a deposition temperature of 80°C, the crystallite size increases and reaches a maximum value of about 22.6429 nm. The decrease in crystallite size initially can be attributed to the weakening force between crystals, possibly due to the substrate remaining in the solution longer than necessary (Braiek *et al.*, 2015) As expected, the increase in crystallite size with the rise in deposition temperature is due to a higher number of Pb and O ions being adsorbed on the substrate, leading to enhanced crystallization. The deposition temperature significantly impacts the deposition rate by increasing the diffusion coefficient of ions and the solubility of the precursor (Mahalingam *et al.*, 2007). It is observed from **Figure 3b** that both dislocation density and micro-strain have a significant impact on the deposition temperature. Both dislocation density and micro-strain reach a slightly higher value at 60°C compared to the deposition temperature at 30°C. However, there is a substantial decrease in the value of both dislocation density and micro-strain when the deposition temperature reaches 80°C. The values of dislocation density and micro-strain increase from 30°C to 60°C, possibly due to a decrease in the forces between the crystals such as Vander-Waals Forces, leading to an increase in grain boundaries (Braiek *et al.*, 2015). As the deposition temperature continues to rise, it relieves the stresses accumulated in the layers, resulting in a significant reduction in dislocation density and micro-strain (Mahalingam *et al.*, 2007), (Begum *et al.*, 2012).When the deposition temperature is increased from 30°C to 60°C, the crystallite size decreases, possibly due to an increase in lattice defects which, in turn, increases the interplanar spacing, dislocation density, and micro-strain in the deposited films. Finally, an increase in the deposition temperature from 60°C to 80°C leads to an increase in the deposition rate, the release of layer-to-layer stresses, and a reduction in grain boundaries, resulting in a decrease in interplanar spacing, dislocation density, micro-strain, and an increase in the crystallite size. Moreover, the low values of interplanar spacing, dislocation density, and micro-strain indicate the high quality of the thin film crystal structure (Mahalingam *et al.*, 2007), (Kocyigit *et al.*, 2019), (Braiek *et al.*, 2015), (Begum *et al.*, 2012).

3.2 Compositional analysis

To study the impact of deposition temperature on compositional and morphological structure, we conducted Energy Dispersive Analysis of X-ray (EDAX) and Electron Scanning Microscopy (SEM). The EDAX findings are presented in **Table 2**:

Table 2. The tabulated EDAX data representation at deposition temperature 30°C, 60°C, and 80°C respectively.

Temp. (°C) →	30 °C				60 °C				80 °C			
Element ↓	Mass (%)	Atom (%)	Ratio (Mass) (%)	Ratio (Atom) (%)	Mass (%)	Atom (%)	Ratio (Mass) (%)	Ratio (Atom) (%)	Mass (%)	Atom (%)	Ratio (Mass) (%)	Ratio (Atom) (%)
Pb	71	40.35	8.76	0.67	58.38	39.77	8.54	0.66	78.88	39.58	8.37	0.65
O	8.1	59.65			6.83	60.23			9.42	60.42		

The graphical representation of the Mass (%) of Pb and O vs. deposition temperature is shown in **Figure 4a.** According to the EDAX data, the Mass (%) of Pb and O decreases at 60˚C compared to 30˚C. Subsequently, the Mass (%) of Pb increases significantly, while the Mass (%) of O increases slightly at 80˚C.

(a)   (b)   (c)
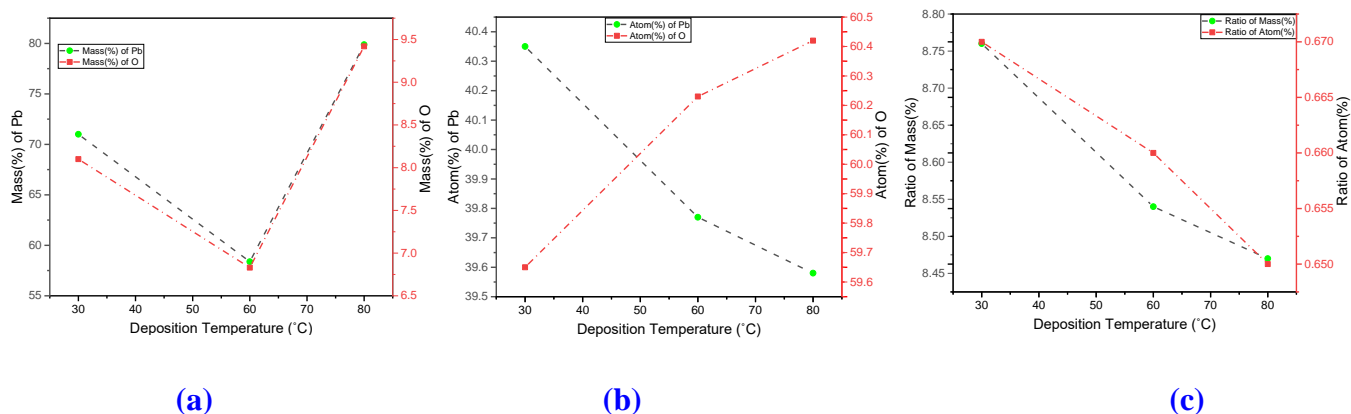
Figure 4. Graphical representation of (**a**) Mass (%) of Pb and O (**b**) Atoms (%) of Pb and O, and (**c**) Ratio of Mass (%) and Atom(%) vs. Deposition temperature.

The graphical representation of Atom (%) of Pb and O vs. deposition temperature is shown in **Figure 4b**. Based on the EDAX data, the Atom (%) of Pb decreases as the deposition temperature rises from 30˚C to 80˚C, while the Atom (%) of O increases. Ultimately, the Atom (%) of Pb decreases significantly, whereas the Atom (%) of O shows a slight increase. Contrary results have been documented for the PbO_2 electrodeposited from nitrate electrolyte (Mahalingam *et al.*, 2007). It can be observed from **Figure 4c** that both the ratio of Atom (%) and Mass (%) decreases with the increase of deposition temperature.

3.3 Morphological Studies

The SEM reveals a stellar, densely minutely tuberculate structure of PbOx deposited at 30˚C temperature, as shown in **Figure 5a-b**. A similar morphology has been reported previously (Mahalingam *et al.*, 2007), (Jayanthi *et al.*, 2018) The tuberculate structure is composed of nanorods, with numerous clusters visible on their surface (Ancevm *et al.*, 2006), as depicted in **Figure 5c**.

(a)   (b)   (c)
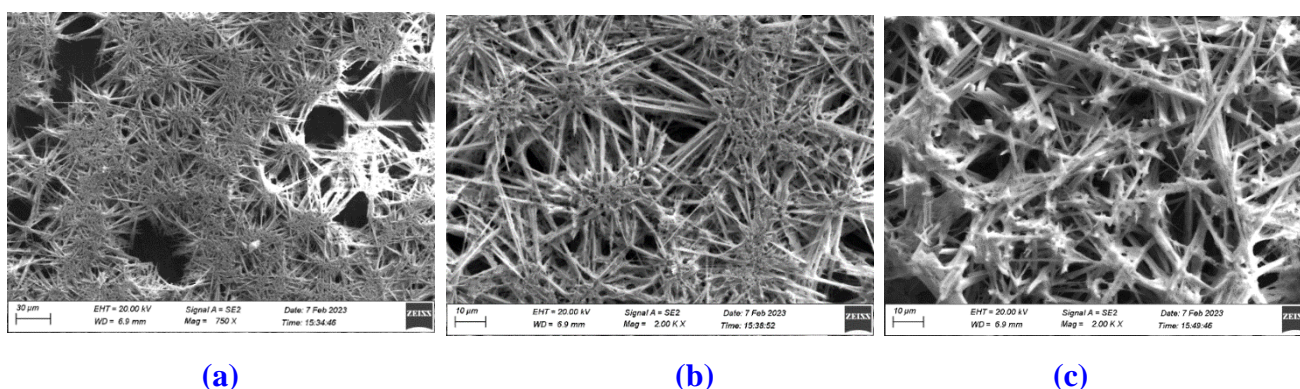
Figure 5a-b. SEM image of PbOx on the copper substrate, which contains stellar structure deposited at 30˚C temperature. **5c** SEM image of PbOx nanorods with some clusters left on the surface of nanorods deposited at 30˚C temperature.

When the temperature rises to 60°C, the nucleation rate increases as well. Consequently, the stellar structure's shape diminishes, and the growth rate significantly rises (Jayanthi *et al.*, 2018), (Ancevm *et al.*, 2006), as depicted in **Figure 6a**. The nanorods exhibit random orientation due to the elevated temperature and still have clusters on their surface (Li *et al.*, 2010), as shown in **Figure 6b-c**. The EDAX analysis also indicates a decrease in the amount of Pb under the previous conditions. Conversely, the amount of O in the composition of PbOx rises at 60°C temperature.

(a) **(b)** **(c)**
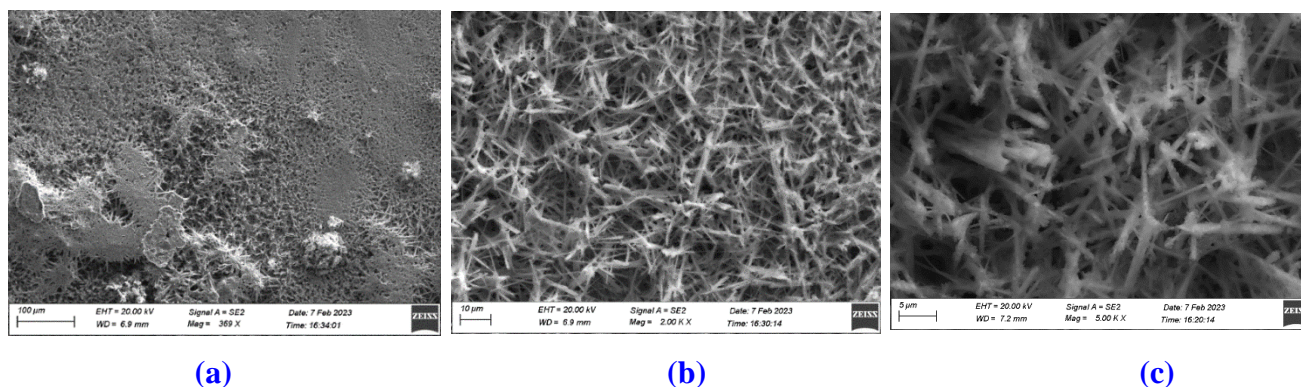
Figure 6a. SEM image of PbOx, which also contain the stellar structure deposited at 60°C temperature. **6b-c.** SEM image of PbOx deposited at 60°C temperature, due to the increase in temperature, the nanorods are randomly orientated, and clusters are also present on the surface.

Two types of morphological structures are observed at 80°C temperatures: stellar and agglomerated fractal structures (Masood *et al.*, 2012), (Khan *et al.*, 2017) as shown in **Figure 7a-b**. These structures form at high temperatures due to the rapid nucleation rate and the random aggregation of Pb and O ions around the working electrode before being deposited. Additionally, stellar structure nanorods are present without any clusters on their surface, as depicted in **Figure 7c**. Furthermore, the EDAX results indicate a decrease in the amount of Pb compared to the previous condition, while the amount of O in the composition of PbOx increases with a rise in temperature to 80°C.

(a) **(b)** **(c)**
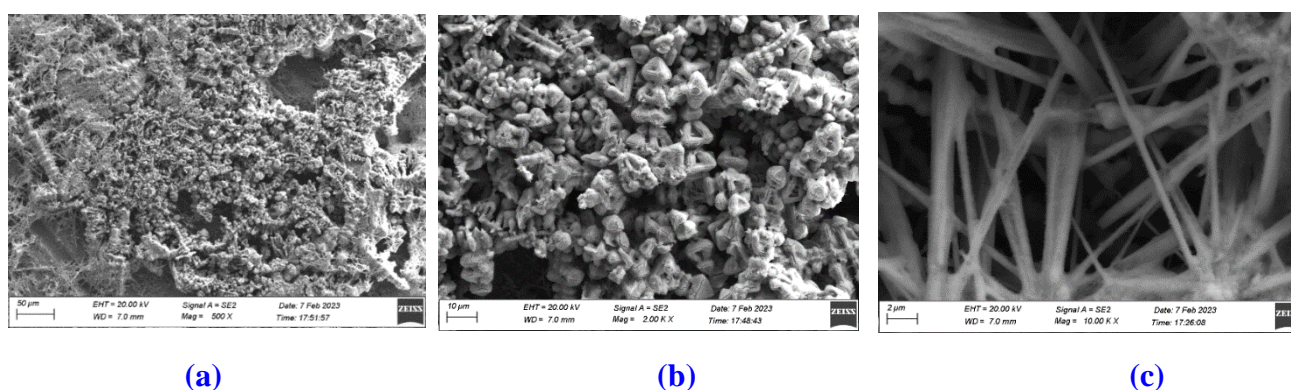
Figure 7a-b. SEM image of PbOx, which also contains the staller as well as fractal structure deposited at 80°C temperature, and **7c** SEM image of PbOx nanorods with no clusters left on the surface of nanorods deposited at 80°C temperature.

Conclusion

The electrochemical deposition of PbOx on a Cu substrate was conducted at three different temperatures at pH-3. Analysis of PbOx through XRD, EDAX, and SEM shows that the deposition temperature significantly impacts the crystalline, compositional, and morphological structure of PbOx

on the Cu substrate. By adjusting the deposition temperature, various properties of electrochemically deposited PbOx can be customized, which is crucial for its diverse applications.

Disclosure statement: *Conflict of Interest:* The authors declare that there are no conflicts of interest.
Compliance with Ethical Standards: This article does not contain any studies involving human or animal subjects.

References

Ai S., Wang Q., Li H., Jin L. (2005) Study on production of free hydroxyl radical and its reaction with salicylic acid at lead dioxide electrode, *Journal of Electroanalytical Chemistry*, 578 (2), 223-229, https://doi.org/10.1016/j.jelechem.2005.01.002.

Al Katrib M., Perrin L., Planes E. (2021) Development of a Perovskite Deposition Method Compatible with Large Surface Covering: Impact of Electrodeposition Parameters, Substrate Nature and Conversion Route. *IEEE 48th Photovoltaic Specialists Conference (PVSC), USA, pp.* 0741-0744, https://doi: 10.1109/PVSC43889.2021.9518447.

Ancev M., Goranova V. (2006) Trichome Morphology of Eleven Genera of the Tribe Alysseae (Brassicaceae) Occurring in Bulgaria, *Willdenowia*, 36(1), 115-123, https://www.jstor.org/stable/3997694.

Begum A., Hussain A., Rahman A. (2012) Effect of deposition temperature on the structural and optical properties of chemically prepared nanocrystalline lead selenide thin films, *Beilstein J. Nanotechnol*, 3, 438–443, https://doi.org/10.3762/bjnano.3.50.

Blood P. J., Brown I. J., Sotiropoulos S. (2004) Electrodeposition of lead dioxide on carbon substrates from a high internal phase emulsion (HIPE), *Journal of Applied Electrochemistry,* 34, 1-7, https://doi.org/10.1023/B:JACH.0000005612.69468.e7.

Braiek Z., et al. (2015) Correlation between physical properties and growth mechanism of In2S3 thin films fabricated by electrodeposition technique with different deposition times, *Eur. Phys. J. Appl. Phys.*, 72(1), 10302, https://doi.org/10.1051/epjap/2015150195.

Boubatra M., et al. (2011) The Influence of pH Electrolyte on the Electrochemical Deposition and Properties of Nickel Thin Films, *Ionics*, 17 (4), 361-369, https://doi.org/10.1007/s11581-011-0642-3.

Braiek Z., et al., (2015) Correlation between physical properties and growth mechanism of In2S3 thin films fabricated by electrodeposition technique with different deposition times, *Eur. Phys. J. Appl. Phys.*, 72 (1), 10302, https://doi.org/10.1051/epjap/2015150195.

Chen H., Wei Z., Zheng X., Yang S. (2015) A Scalable Electrodeposition Route to the Low-Cost, Versatile and Controllable Fabrication of Perovskite Solar Cells, *Nano Energy*, 15, 216-226, https://doi.org/10.1016/j.nanoen.2015.04.025.

Chen T., Huang H., Ma H., Kong D. (2013) Effect of Surface Morphology of Nanostructured PbO_2 Thin Films on their Electrochemical Properties, *Electrochimica Acta*, 88, 79-85, https://doi.org/10.1016/j.electacta.2012.10.009.

Devilliers D., Dinh Thi M. T., Mahé E., Le Xuan Q. (2003) Cr(III) oxidation with lead dioxide-based anodes, *Electrochimica Acta*, 48(28), 4301-4309, https://doi.org/10.1016/j.electacta.2003.07.005.

Duan X., Zhao C., Liu W., Zhao X., Chang L. (2017) Fabrication of a novel PbO_2 electrode with a graphene nanosheet interlayer for electrochemical oxidation of 2-chlorophenol, *Electrochim. Acta,* 240, 424–436, https://doi.org/10.1016/j.electacta.2017.04.114.

Eftkhari A. (2003), pH sensor based on the deposited film of lead oxide on aluminum substrate electrode, *Sensors and Actuators B: Chemical*, 88(3), 234-238, https://doi.org/10.1016/S0925-4005(02)00321-0.

Elaissaoui I., Akrout H., Grassini S., Fulginiti D., Bousselmi L. (2018) Effect of coating method on the structure and properties of a novel PbO_2 anode for electrochemical oxidation of Amaranth dye, *Chemosphere*, 10, 161-168. doi: https://doi.org/10.1016/j.chemosphere.2018.10.161.

Hossain M. D., et al. (2017) Effect of Deposition Parameters on the Morphology and Electrochemical Behavior of Lead Dioxide, *Journal of Electrochemical Science and Technology*, 8(3), 197-205, https://doi.org/10.33961/JECST.2017.8.3.197.

Jayanthi P. D. K., et al. (2018) Morphological Diversity of Trichomes and Phytochemicals in Wild and Cultivated Eggplant Species *Indian Journal of Horticulture*, 75(2), 265-271, https://doi.org/10.5958/0974-0112.2018.00045.2.

Johnson D. C., Feng J., Houk L. L. (2000) Direct electrochemical degradation of organic wastes in aqueous media, *Electrochimica Acta*, 46(2-3), 323-330, https://doi.org/10.1016/S0013-4686(00)00588-0.

Kinoshita K. (1992) *Electrochemical oxygen technology,* John Wiley & Sons, New York, ISBN: 978-0-471-57043-1.

Khan S. A., Shahid S., Ijaz F. (2017) *Green Synthesis of Copper oxide Nanoparticles & Biomedical Application*, *1st ed.*, Lambert Academic Publishing, ISBN: 978-620-2-02718-2.

Kocyigit A., Topkaya R. (2019) Structural, optical and magnetic properties of Ni-Co co-doped ZnO thin films, *Materials Research Express*, 6(9), 096116, https://doi.org/10.1088/2053-1591/ab120a.

Labiadh L., Barbucci A., Carpanese M. P., Gadri A., Ammar S., Panizza M. (2016) Comparative depollution of Methyl Orange aqueous solutions by electrochemical incineration using $TiRuSnO_2$, BDD and PbO_2 as high oxidation power anodes, *J. Electroanal. Chem.,* 766, 94-99, https://doi.org/10.1016/j.jelechem.2016.01.036.

Li S., et al. (2010) Anisotropic Growth of Iron Oxyhydroxide Nanorods and Their Photocatalytic Activity, *Adv. Eng. Mater.*, 12(10), 1082-1085, https://doi.org/10.1002/adem.201000081.

Mahalingam T., Thanikaikarasan S., Chandramohan R., Raja M., Sanjeeviraja C., Kim J-H., Kim Y. D. (2007) Effects of bath temperature in electrodeposited FeSe2 thin films, *Materials Chemistry and Physics*, 106(2-3), 369-374, https://doi.org/10.1016/j.matchemphys.2007.06.014.

Mahalingam T., et. al. (2007) Electrosynthesis and characterization of lead oxide thin films, *Mat. Characteriz.* 58(8-9), 817-822, https://doi.org/10.1016/j.matchar.2006.11.021.

Masood S., et al. (2012) Copper Fractal Growth Pattern in Polymer Systems, *Int'l. J, Chem.*, 4(6), 15-22, https://doi.org/10.5539/ijc.v4n6p15.

Nikolic´ N. D., et al. (2013) Influence of the complex formation on the morphology of lead powder particles produced by the electrodeposition processes *Adv. Powder Tech,* 24(3), 674-682, http://dx.doi.org/10.1016/j.apt.2012.12.008.

Nikolić N. D., Pavlović L. J., Pavlović M. G., Popov K. I. (2007) Effect of temperature on the electrodeposition of disperse copper deposits, *J. Serb. Chem. Soc.*, 72(12), 1369-1381, https://doi.org/10.2298/JSC0712369N.

Panizza M., Cerisola G. (2003) Influence of anode material on the electrochemical oxidation of 2-naphthol Part 1. Cyclic voltammetry and potential step experiments, *Electrochimica Acta*, 48(23), 3491-3497, https://doi.org/10.1016/S0013-4686(03)00468-7.

Pletcher D., Walsh F. C. (1993) *Industrial Electrochemistry, 2nd edn*, Springer Dordrecht, https://doi.org/10.1007/978-94-011-2154-5.

Sáez V., et al. (2011) Lead dioxide film sonoelectrodeposition in acidic media: Preparation and performance of stable practical anodes, *Ultrasonics Sonochemistry*, 18(4), 873–880, https://doi.org/10.1016/j.ultsonch.2010.11.018.

Salim T., et al. (2015) Perovskite-Based Solar Cells: Impact of Morphology and Device Architecture on Device Performance, *J. Mater. Chem. A*, 3(17), 8943-8969, https://doi.org/10.1039/C4TA05226A.

Stillman R. et al. (1984) Quantitative X-Ray Diffraction Analysis of A-Pbo/Fl-Pbo in Lead-Acid Battery Primary Oxide, *Journal of Power Sources*, 13, 171-180, https://doi.org/10.1016/0378-7753(84)80001-4.

Stucki S., Theis G., Kötz R., Devantay H., Christen H. J. (1985) In situ production of ozone in water using a Membrel electrolyzer, *Journal of the Electrochemical Society*, 132(2), 367-371, https://doi.org/10.1149/1.2113840.

Suganya M., Balu A. R., and Usharani K. (2014), Role of substrate temperature on the growth mechanism and

physical properties of spray deposited lead oxide thin films, *Materials Science-Poland*, 32(3), 448-456, https://doi.org/10.2478/S13536-014-0208-y.

Tang Y., Chen Z., Jia Z., Zhang L., Li J. (2005) Electrodeposition and characterization of nanocrystalline cuprous oxide thin films on TiO_2 films, *Materials Letters*, 59(4), 434-438, https://doi.org/10.1016/j.matlet.2004.09.040.

Tong S.-P., Ma C.-A., Feng H. (2008) A Novel PbO_2 Electrode Preparation and Its Application in Organic Degradation, *Electrochimica Acta*, 53(6), 3002-3006, https://doi.org/10.1016/j.electacta.2007.11.011.

Zhao X., Li C., Wang Y., Xu W. (2018) Electrodeposited PbO_2 Thin Films with Different Surface Structure as Position Plant in Lead Acid Batteries, *Int. J. Electrochem. Sci.*, 13, 3745-3756, https://doi.org/10.20964/2018.04.52.